

See discussions, stats, and author profiles for this publication at: <https://www.researchgate.net/publication/51770382>

Triazole-Linked-Thiophene Conjugate of Calix[4]arene: Its Selective Recognition of Zn²⁺ and as Biomimetic Model in Supporting the Events of the Metal Detoxification and Oxidative S...

ARTICLE *in* THE JOURNAL OF ORGANIC CHEMISTRY · NOVEMBER 2011

Impact Factor: 4.72 · DOI: 10.1021/jo201865x · Source: PubMed

CITATIONS

22

READS

146

4 AUTHORS, INCLUDING:



Rakesh Pathak

University of Georgia

25 PUBLICATIONS 342 CITATIONS

[SEE PROFILE](#)



Milon Mondal

University of Groningen

7 PUBLICATIONS 53 CITATIONS

[SEE PROFILE](#)

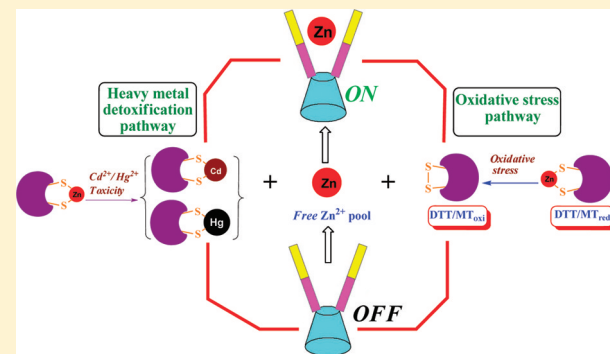
Triazole-Linked-Thiophene Conjugate of Calix[4]arene: Its Selective Recognition of Zn²⁺ and as Biomimetic Model in Supporting the Events of the Metal Detoxification and Oxidative Stress Involving Metallothionein

Rakesh Kumar Pathak,[†] Vijaya Kumar Hinge,[‡] Milon Mondal,[†] and Chebrolu Pulla Rao^{*,†,‡}

[†]Bioinorganic Laboratory & Department of Chemistry and [‡]Department of Biosciences & Bioengineering, Indian Institute of Technology Bombay, Powai, Mumbai 400 076, India

Supporting Information

ABSTRACT: Supramolecular calix[4]arene conjugate (**L**) has been developed as a sensitive and selective sensor for Zn²⁺ in HEPES buffer among the 12 metal ion by using fluorescence, absorption and ESI MS and also by visual fluorescent color. The structural, electronic, and emission properties of the calix[4]arene conjugates **L** and its zinc complex, [ZnL], have been demonstrated using *ab initio* density functional theory (DFT) combined with time-dependent density functional theory (TDDFT) calculations. The TDDFT calculations reveal the *switch on* fluorescence behavior of **L** is mainly due to the utilization of the lone pair of electrons on imine moiety by the Zn²⁺. The resultant fluorescent complex, [ZnL], has been used as a secondary sensing chemo-ensemble for the detection of –SH containing molecules by removing Zn²⁺ from [ZnL] and forming {Cys/DTT·Zn} adducts as equivalent to those present in metallothioneins. The displacement followed by the release of the coordinated zinc from its Cys/DTT complex by heavy metal ion (viz. Cd²⁺ and Hg²⁺), as in the metal detoxification process or by ROS (such as H₂O₂) as in the oxidative stress, has been well demonstrated using the conjugate **L** through the fluorescence intensity retrieval wherein the fluorescence intensity is the same as that observed with [ZnL], which in turn mimics the zinc sensing element (MTF) in biology.



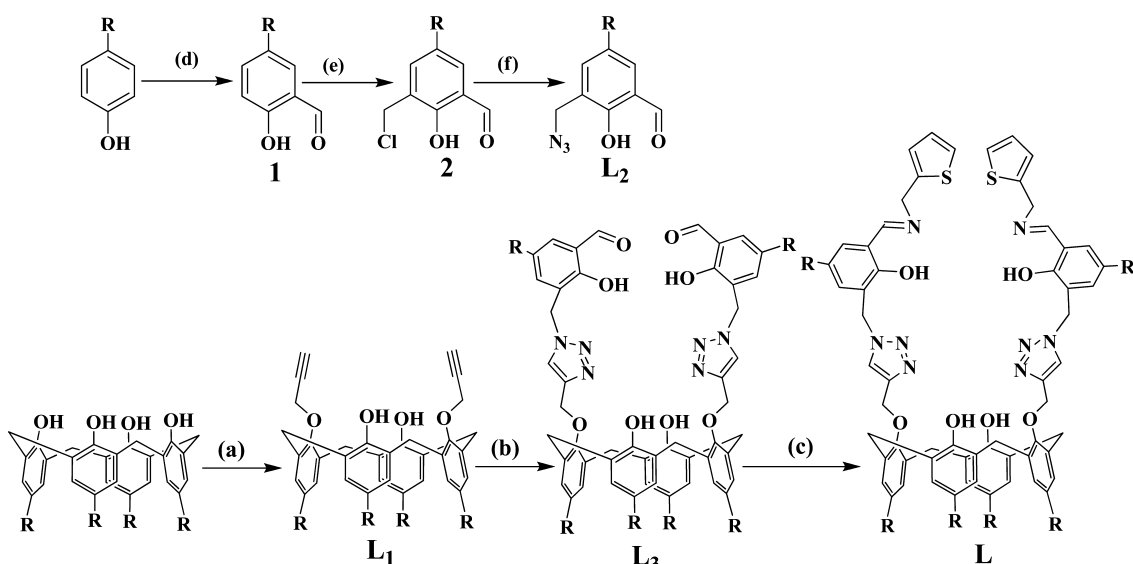
INTRODUCTION

Metallothioneins (MTs) are low-molecular-weight proteins having high cysteine content and thereby exhibit strong ability to complex metal ions with greater affinity being imparted toward softer ones.¹ Two most important functions of MTs are the heavy metal detoxification and antioxidant property.² These are controlled by the free and loosely bound zinc ions.^{2,3} The reactive oxygen species (ROS) induced oxidation of thiols triggers the formation of the oxidized protein thionine (T_{ox}) with the concomitant release of Zn²⁺.⁴ In the presence of toxic heavy metal ions, Cd²⁺ and Hg²⁺ bind strongly with the MT_{red} by replacing Zn²⁺ and therefore hinder the process of oxidative stress and other enzymatic pathways.⁵ At this stage, the concentration of Zn²⁺ increases in the cytosol and the elevated levels of free zinc binds to the metal-regulatory transcription factor (MTF), thus inducing the expression of thionine, and the expressed MT_{red} state is stabilized by the Zn²⁺ through binding.^{3,6} A molecular mechanistic based knowledge of the release of Zn²⁺ from the Cys rich binding domains of MT_{red} is expected to demonstrate the bioinorganic pathways of these events. Synthetic fluorescent conjugates which selectively recognize Zn²⁺ can be used to demonstrate the events involved in the metal detoxification and the oxidative stress.⁷ In the

recent times, supramolecular calixarene conjugates have been evolving as mimics for metalloproteins and metalloenzymes.^{8,9} Upon appropriate derivatization, the conjugates of calix[4]-arene can be tuned to be sensitive and selective toward certain metal ion.¹¹ Therefore, the synthetic conjugates of calix[4]-arene which senses Zn²⁺ selectively can be of great advantage^{10–12} in this, while sulfhydryl bearing small organic molecules, such as cysteine (Cys) and dithiothreitol (DTT), can act as MT mimics.¹³ Hence, in the present paper we report the synthesis, characterization of thiophene appended triazole-linked calix[4]arene conjugate, **L**, and its selective recognition behavior toward Zn²⁺. The structural, electronic, and emission properties of the calix[4]arene conjugate **L** and its zinc complex, [ZnL], have been demonstrated using *ab initio* density functional theory (DFT) along with the calculations of the time-dependent density functional theory (TDDFT). Furthermore, this conjugate has been demonstrated as a biomimetic model system to support the events involved in the oxidative stress and metal detoxification pathways through the sensitive and selective recognition of Zn²⁺.

Received: September 10, 2011

Published: November 4, 2011

Scheme 1. Synthesis of the Precursor Molecule, L₂, and the Final Receptor Molecule, L^a

^aSynthesis of receptor L: (a) propargyl bromide, K₂CO₃, acetone, reflux, 24 h, 82%; (b) 5-tert-butyl-3-(azidomethyl)-2-hydroxybenzaldehyde (L₂), CuSO₄·5H₂O and sodium ascorbate in dichloromethane: water (1:1) rt, 12 h, 89.9%; (c) thiophene-2-ylmethanamine, methanol, rt, 8 h, 93%; (d) SnCl₄, Bu₃N, (CH₂O)_n, dry toluene, reflux, 63%; (e) 37% formaldehyde, concentrated HCl, rt, 24 h, 82%; (f) NaN₃, DMF, rt, 12 h, 89%. R = *tert*-butyl.

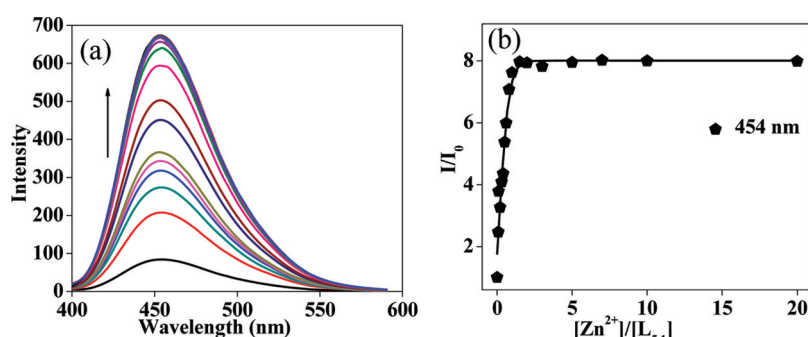


Figure 1. (a) Fluorescence spectra obtained during the titration of L with Zn²⁺ in aqueous ethanol (1:2 v/v) HEPES buffer (pH = 7.4), $\lambda_{\text{ex}} = 390$ nm, [L] = 10 μM . (b) Relative fluorescence intensity (I/I_0) as a function of $[\text{Zn}^{2+}]/[\text{L}]$ mole ratio.

RESULTS AND DISCUSSION

The calix[4]arene conjugate, L, was synthesized by going through three consecutive steps^{11h} starting from *p*-*tert*-butylcalix[4]arene followed by the preparation of its dipropargyl ether and triazole linked conjugate as shown in Scheme 1. The copper(I)-catalyzed 1,3-dipolar cycloaddition reaction was used for the introduction of L₂ onto the calixarene scaffold. The precursor azide derivative L₂ has been synthesized in three steps,^{11h,14} starting from the *p*-*tert*-butylphenol (Scheme 1). The final receptor molecule has been synthesized by the condensation of the L₃ with thiophene methylamine as shown in Schemes 1. All the precursor and receptor molecules were characterized by various analytical and spectral techniques, and the calix[4]arene conjugates were found to be in cone conformation as per the data given in the Experimental Section as well as in the Supporting Information, Figures S1–S4.

A. Metal Ion Recognition Studies. In order to understand the selective and sensitive metal ion binding behavior of L, fluorescence and absorption titrations were carried out.

Fluorescence Studies. The receptor L exhibits weak fluorescence emission at \sim 454 nm owing to the photoelectron transfer when excited at 390 nm in 1:2 HEPES buffer:ethanol

mixture at pH = 7.4. Titration of L with Zn²⁺ results in the enhancement of the fluorescence intensity as a function of the added Zn²⁺ concentration (Figure 1a) and the intensity saturates at \geq 1 equiv. The *switch on* fluorescence emission is expected to the reversal of photoelectron transfer (PET) upon utilization of the lone pair of electrons on imine moiety by the Zn²⁺. A plot of the fluorescence intensity vs [Zn²⁺]/[L] mole ratio (Figure 1b) fits well with the formation of a 1:1 stoichiometric complex between L and Zn²⁺, and the binding constant derived from the Benesi–Hildebrand equation was found to be $(9.2 \pm 0.2) \times 10^{-4} \text{ M}^{-1}$. The observed high K_a value clearly indicates the strong affinity of Zn²⁺ to L. In order to check whether the L is sensitive to only Zn²⁺ or even to the other ions, similar fluorescence titrations were carried out in the same medium with 11 other different metal ions, viz. Na⁺, K⁺, Mg²⁺, Ca²⁺, Mn²⁺, Fe²⁺, Co²⁺, Ni²⁺, Cu²⁺, Cd²⁺, and Hg²⁺, and found no significant fluorescence enhancement in the presence of any of these ions (Figure 2).

Therefore, L is selective to Zn²⁺ among the 12 ions studied. Visual fluorescent color change experiments have been carried out to look at the behavior of L in the presence of various metal ions. Under UV light, the solution of L is nonfluorescent,

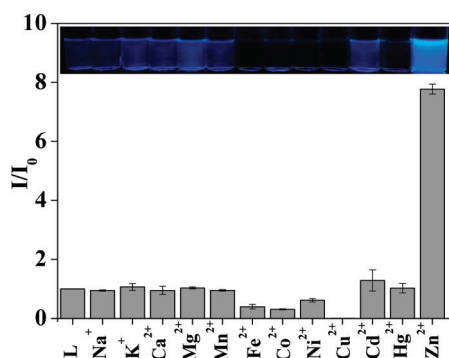


Figure 2. Histogram showing the relative fluorescence response of **L** in the presence of different metal ions, $[L] = 10 \mu\text{M}$. The inset shows the visual fluorescent color change of **L** in presence of these ions under 365 nm incident light.

whereas in the presence of Zn^{2+} , it shows an intense blue fluorescent color which is otherwise not present in case of the other metal ions studied (Figure 2 inset). Therefore, Zn^{2+} can easily be differentiated by visual color change among the other metal ions.

The sensitivity of **L** for Zn^{2+} has been further evaluated by measuring the lowest concentration that can be determined. The fluorescence titration carried out between **L** and $[\text{Zn}^{2+}]$ by maintaining a 1:1 ratio gives a value of $47 \pm 8 \text{ ppb}$ ($718 \pm 122 \text{ nM}$), suggesting its applicability to detect Zn^{2+} ions in aqueous medium at physiological conditions. To our knowledge, this is one of those few calix[4]arene conjugates which possess high sensitivity toward Zn^{2+} in the literature that can quantify Zn^{2+} even below 100 ppb level (Supporting Information, Figure S5). Therefore, **L** can be used as a sensitive and selective *in vitro* receptor for Zn^{2+} .

Competitive Metal Ion Titration. In order to show the practical utility of **L** to detect Zn^{2+} selectively even in the presence of other metal ions, competitive metal ion titrations were carried out. These studies reveal that the Zn^{2+} -induced fluorescence enhancement was unaffected in the presence of biologically relevant alkali (Na^+ , K^+), alkaline earth (Mg^{2+} and Ca^{2+}), first row transition (Mn^{2+} , Fe^{2+} , Co^{2+} , Ni^{2+}), and the toxic metal ions (Cd^{2+} and Hg^{2+}). However, this is completely quenched in the presence of Cu^{2+} . Thus, it is notable that **L** can be used as a selective Zn^{2+} fluorescent sensor in the presence of most of the metal ions (Figure 3), except Cu^{2+} .

Absorption Titrations with Zn^{2+} . Absorption titrations were carried out in aqueous ethanol (1:2 v/v) HEPES buffer ($\text{pH} = 7.4$) to support the binding of Zn^{2+} with **L**. The absorption spectra of free **L** ($10 \mu\text{M}$) exhibits bands at ~ 325 and ~ 435 nm. Upon the addition of Zn^{2+} , the new band observed at ~ 380 nm shows increased absorbance, while that of the other two bands at ~ 325 and ~ 435 nm show decrease. The isosbestic points observed at 345 and 415 nm were indicative of the transition between the unbound **L** and its Zn^{2+} complexed species (Figure 4). The stoichiometry of the complex formed between **L** and Zn^{2+} has been further shown to be 1:1 by the Job's plot (Supporting Information, Figure S6).

Electrospray Mass Spectrometry. ESI MS spectrum obtained for the titration of **L** with Zn^{2+} results in a molecular ion peak at $m/z = 1443.62$ that corresponds to $[\text{L} + \text{Zn} + \text{H}]^+$. The isotopic peak pattern observed is characteristic for the presence of zinc supporting the complex formation (Supporting Information, Figure S7) of **L** with Zn^{2+} (Figure 5).

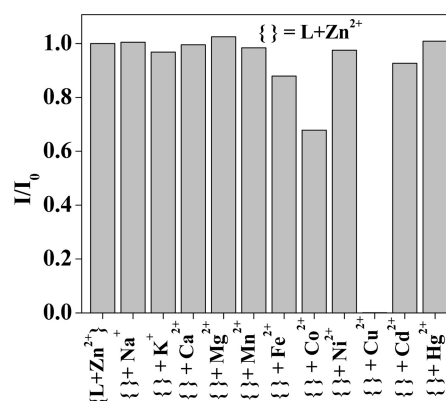


Figure 3. Histogram showing the fluorescence response of **L** with Zn^{2+} in the presence of various metal ion in aqueous ethanol (1:2 v/v) HEPES buffer ($\text{pH} = 7.4$) solution. $[L] = 10 \mu\text{M}$, 2 equiv of Zn^{2+} , and 5 equiv of other metal ions have been used.

NMR Titrations of **L with Zn^{2+} .** In order to support the formation of the complex between **L** and Zn^{2+} , ^1H NMR titrations were carried out. During the titration, the concentration of **L** was kept constant and the added $[\text{Zn}^{2+}]$ mole ratio was varied, viz. 0, 0.5, 1, 1.5, 2.0, and 3.0 equiv (Figure 6). Upon the interaction of **L** with Zn^{2+} , the chemical shifts of the protons of imine, thiophene, salicyl, and bridged $-\text{CH}_2$ showed marginal to considerable changes and that of the salicylic–phenolic-OH disappears within 1 equiv. The absence of any significant changes in the chemical shift of the triazole proton rules out the interaction between this moiety and the Zn^{2+} . The considerable shift observed in the thiophene- CH_2 , salicyl-H, and thiophene-H supports the role of salicylimine–thiophene core in the Zn^{2+} binding. The ^{13}C NMR spectra of **L** and $[\text{L} + 2 \text{ equiv } \text{Zn}^{2+}]$ have been compared and found to have significant spectral differences supporting the complex formation (Supporting Information, Figure S8).

Structural Features of $[\text{ZnL}]$ by Computational Methods. As no structure could be established for the zinc complex due to its noncrystallinity, though the precursor **L** was crystalline (Supporting Information, Figure S9), DFT-based calculations were performed to understand the structural and coordination features of $[\text{ZnL}]$ complex. Therefore, both **L** and $[\text{ZnL}]$ were optimized by DFT using Gaussian 03 package¹⁵ as explained in the Experimental Section, and the corresponding ground state structures obtained from DFT calculations are shown in Figure 7. In $[\text{ZnL}]$, Zn^{2+} shows highly distorted tetrahedral geometry, where it is bonded through two salicyl oxygens, imine nitrogens. One of the sulfur of thiophene showed weaker coordination with zinc by a distance of 2.78 \AA , which is higher than the normal thiolate/thioethers-Zn bond distance. Therefore, the interaction between $\text{Zn}\cdots\text{S}$ is of van der Waal's type. When this $\text{Zn}\cdots\text{S}$ interaction is being included in the coordination sphere, the zinc exhibits a distorted square-pyramidal geometry. However, the second thiophene moiety does not participate in binding as the Zn to S distance is 5.13 \AA (Supporting Information, Figures SI-10–SI-14). The natural bonding orbital (NBO) charge analysis shows that a more positive charge on the zinc center and negative charges on the coordinated O and N atoms of $[\text{ZnL}]$ $\{\text{Zn} = 1.26, \text{N}_1 = -0.66, \text{N}_2 = -0.66, \text{O}_1 = -0.76, \text{O}_2 = -0.75\}$. The charge on the zinc center is >1 and indicates more of an interaction of the ionic nature between the metal center and the ligands.

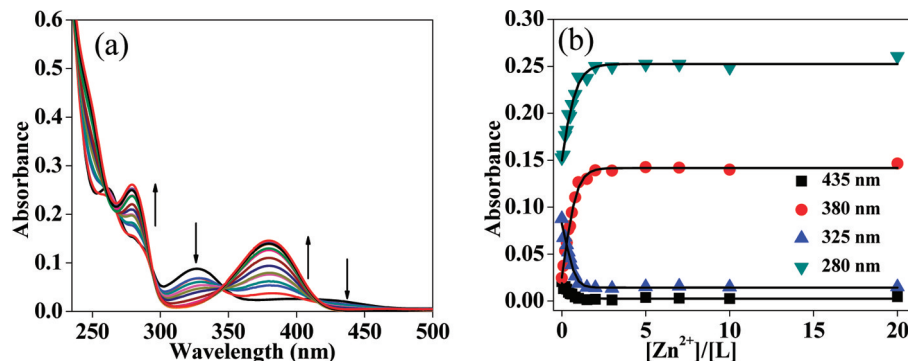


Figure 4. (a) Absorption spectra obtained during the titration L ($10 \mu\text{M}$) with Zn^{2+} in aqueous ethanol (1:2 v/v) HEPES buffer ($\text{pH} = 7.4$). (b) Plot of absorbance vs. $[\text{Zn}^{2+}]/[\text{L}]$ mole ratio for different absorption bands.

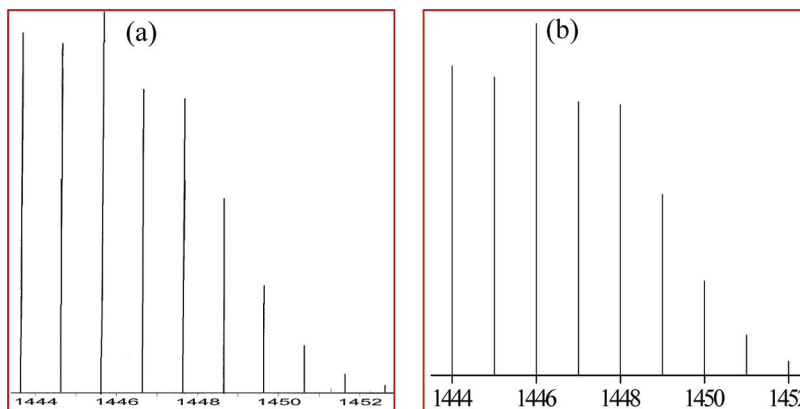


Figure 5. ESI MS spectrum obtained during the titration of L with Zn^{2+} for the 1:1 complex along with its isotopic peak pattern: (a) observed and (b) calculated.

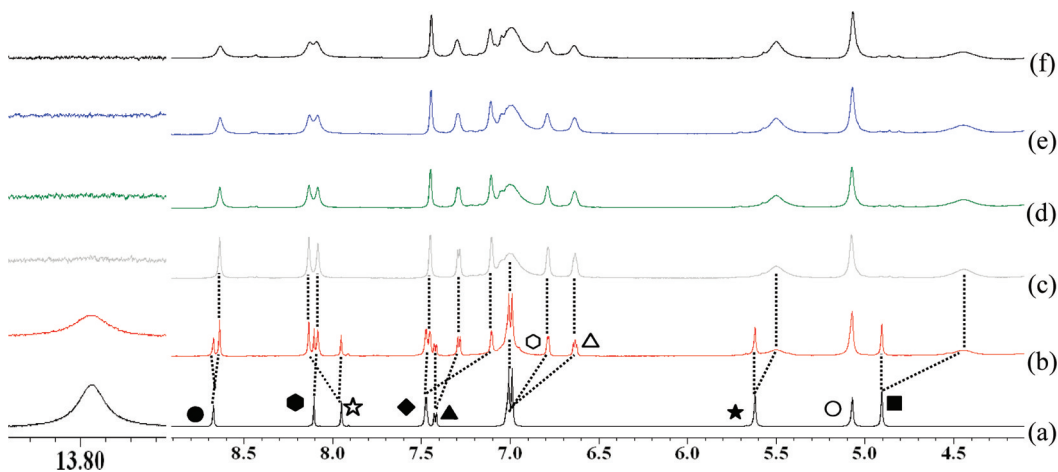


Figure 6. ^1H NMR spectra measured during the titration of L with different mole ratio of Zn^{2+} in $\text{DMSO}-d_6$: (a) 0, (b) 0.5, (c) 1.0, (d) 1.5, (e) 2.0, and (f) 3.0: (●) imine-H; (○, ▲, △) thiophene-H; (★, ○, ■) bridged CH_2 protons.

Calculations based on single-excitation time-dependent density functional theory (TDDFT) were performed to explain the electronic structural properties of the ground and excited states behavior of L and $[\text{ZnL}]$.¹⁶ The vertical transitions calculated by TDDFT (Table 1) were compared (Figure 8) and were found to be in good agreement with the experimental data.

The TDDFT calculations were performed at the B3LYP/6-31G(d,p) level and found to support the absorption bands observed in the region of $\lambda_{\text{max}} = 270\text{--}450 \text{ nm}$. These studies

suggest that the band observed at $\sim 377 \text{ nm}$ corresponds to λ_{max} of UV experimental spectra of $[\text{ZnL}]$ and $\sim 321 \text{ nm}$ corresponds to L. In case of $[\text{ZnL}]$, the observed band at $\sim 377 \text{ nm}$ is assigned to the transition B (Table 1) that results from a $\pi \rightarrow \pi^*$ transition within the salicylimine fragment, which mainly corresponds to two—one electron excitations from 318/HOMO-2 \rightarrow 321/LUMO and 320/HOMO \rightarrow 322/LUMO+1. The corresponding (molecular orbital's) MO's are shown in Figure 9 (Table 1). In Figure 9A, the MO's are majorly localized on salicylimine part of $[\text{ZnL}]$, and the transitions are

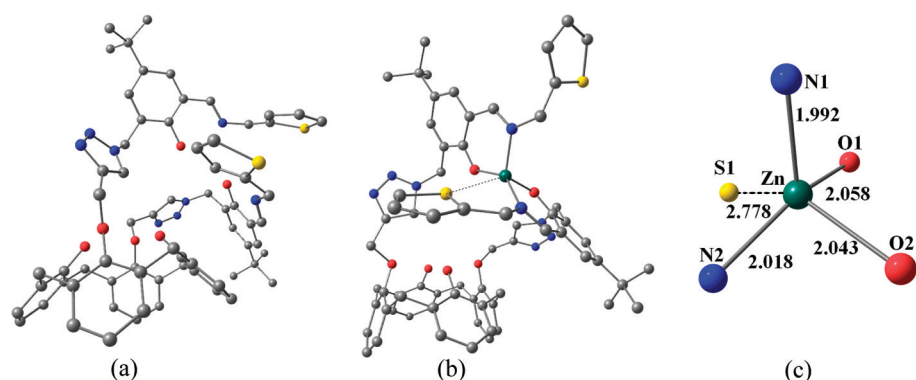


Figure 7. DFT optimized structure of (a) L and (b) $[ZnL]$. Hydrogen's were omitted for the clarity. (c) Coordination sphere around the zinc ion, bond angles (deg) in the coordination sphere are $N_1-Zn-O_1 = 93.5$, $N_1-Zn-O_2 = 111.3$, $N_1-Zn-N_2 = 116.5$, $N_1-Zn-S_1 = 106.4$, $O_1-Zn-O_2 = 92.5$, $O_1-Zn-N_2 = 144.3$, $O_1-Zn-S_1 = 78.3$, $O_2-Zn-N_2 = 93.4$, $O_2-Zn-S_1 = 141.5$, $N_2-Zn-S_1 = 75.1$.

Table 1. Main Singlet Vertical Electron Transition Energies (ΔE), Wavelengths (λ), Oscillator Strengths (F), and Configuration Interaction Coefficients (CI_{coeff}) for $[ZnL]$, Calculated at the TDDFT Level

transition	ΔE [eV] (λ nm)	F	key excited state (CI_{coeff})	contribution (%)	assignment
A	3.2047 (386)	0.0852	HOMO-2 \rightarrow LUMO (0.62332)	78	salicylimine \rightarrow salicylimine ($\pi-\pi^*$)
B	3.2885 (377)	0.1534	HOMO-2 \rightarrow LUMO (0.13094)	78	salicylimine \rightarrow salicylimine ($\pi-\pi^*$)
C	3.4914 (355)	0.0041	HOMO-2 \rightarrow LUMO+1 (0.6988)	98	salicylimine 1 \rightarrow salicylimine 2 ($\pi-\pi^*$)
D	3.9349 (315)	0.0048	HOMO \rightarrow LUMO+2 (0.70082)	98	LMCT

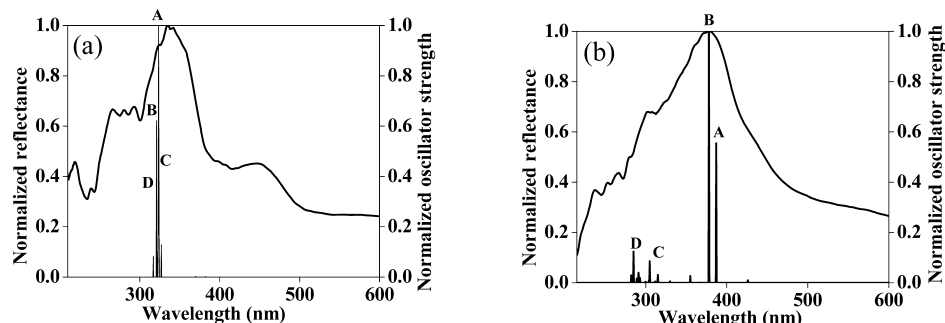


Figure 8. Normalized TDDFT singlet monoelectronic vertical transitions and normalized diffuse reflectance spectrum: (a) L and (b) $[ZnL]$.

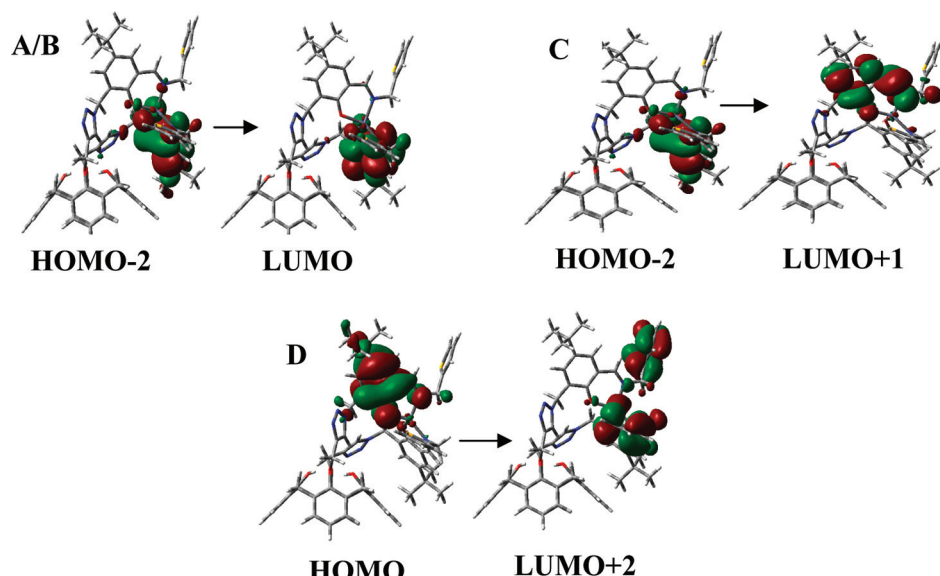


Figure 9. Pictorial representation of the molecular orbital's (MOs) calculated for the singlet vertical electron transitions A to D (given in Table 1) using TDDFT for $[ZnL]$.

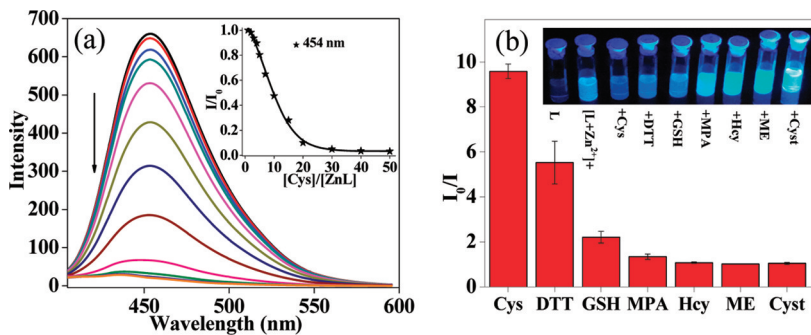


Figure 10. (a) Fluorescence spectra obtained during the titration of $\{L + Zn^{2+}\}$ with Cys in aqueous ethanolic (1:2 v/v) HEPES buffer ($pH = 7.4$), $\lambda_{ex} = 390$ nm. The inset shows the relative fluorescence intensity (I/I_0) as a function of $[Cys]/[ZnL]$ mole ratio. (b) Histogram showing relative fluorescence response of various biological thiols with $[ZnL]$. The inset shows the visual fluorescent color change of $[ZnL]$ in the presence of different $-SH$ -containing molecules, along with controls, under 365 nm incident light.

similar to those observed in B but with a lesser oscillator strength when compared to that in Figure 9B (Table 1). Part C mainly corresponds to the transition from the π MO's of one salicylimine to the π^* MO of the other salicylimine of $[ZnL]$ and corresponds to the pure 318/HOMO-2 \rightarrow 322/LUMO+1 excitation. In case of part D, the ligand-to-metal charge transfer (LMCT) was observed from one of the salicylimine moiety to zinc ion, and the corresponding 320/HOMO and 323/LUMO-2 MO's are given in Figure 9. The TDDFT calculations have been carried out for L and the corresponding electronic transitions details included in the Supporting Information, Figures S11 and S15.

The origin of fluorescence behavior of L in presence of Zn^{2+} can be explained based on the *fluorescence enhancement by orbital control* (FEOC) phenomena.¹⁷ In the present case the fluorescence behavior of L and $[ZnL]$ has been demonstrated on the basis of the involvement of imine-nitrogen lone pair toward Zn^{2+} binding. In L, the major contribution to the excitation is from the nitrogen lone pair, viz. HOMO-3 to LUMO (77%) and HOMO-5 to LUMO (57%), and therefore contributes for the fluorescence quenching (Supporting information, Figures S12 and S13 and Table S4). However, in case of $[ZnL]$, the nitrogen lone pair orbitals are involved in the binding of Zn^{2+} and therefore not available for the excitation transitions which otherwise correspond to the fluorescence quenching. Hence, upon complexation, Zn^{2+} blocks the involvement of nitrogen lone pair in the excitation and thereby enhances the fluorescence of $[ZnL]$.

B. Secondary Sensing of Thiols by L. Thus, L recognizes Zn^{2+} with high selectivity and sensitivity by *switching on* the

fluorescence and forming a 1:1 complex. Therefore, the resulting fluorescent chemo-ensemble zinc complex $[ZnL]$ has been used for the study of the recognition of thiol ($-SH$) bearing molecules, since the ligating centers in metallothionein mainly arise from the side chain $-SH$ function of the Cys residues.

Fluorescence Titrations. The chemosensing ensemble used in these titrations was prepared by *in situ* mixing of L with Zn^{2+} . The *in situ* complex $[ZnL]$ shows strong fluorescence emission at ~ 454 nm when excited at 390 nm. The fluorescence titrations carried out with cysteine (Cys), dithiothreitol (DTT), glutathione reduced (GSH), mercaptoperpropionic acid (MPA), homocysteine (Hcy), mercaptoethanol (ME), and cysteamine (Cyst) all exhibited fluorescence quenching; however, a considerably high quenching was observed mainly in the case of Cys, DTT, and GSH in the order Cys > DTT > GSH (Figure 10), while the others exhibited only minimal changes (Figure 10b), suggesting that the chelatable $-SH$ -containing molecules are effective and not the others (Supporting Information, Figure S14). In fact, the Cys and DTT are good mimics of the Zn^{2+} binding regions of MT_{red} during oxidative stress and heavy metal ion detoxification process. The fluorescence quenching observed in the presence of Cys and DTT may be attributed initially to their interaction with the $[ZnL]$, followed by the removal of Zn^{2+} from this complex, and the chelation of the freed Zn^{2+} by Cys and DTT. All these suggests that the chelating ability of the $-SH$ molecules is

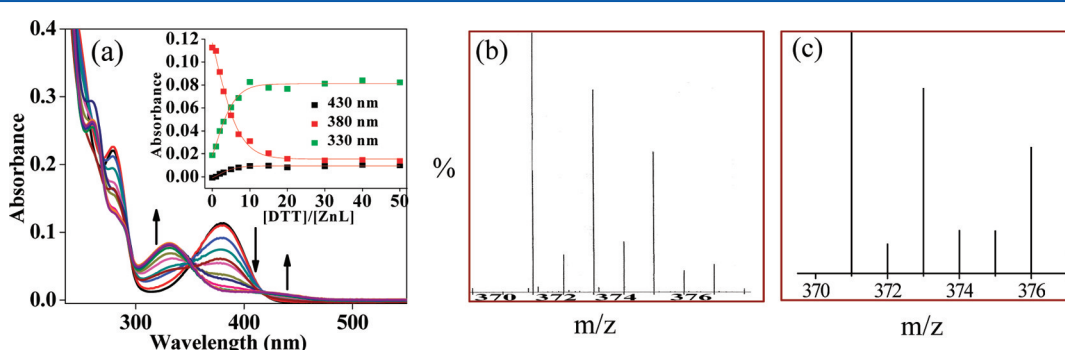


Figure 11. (a) Absorption spectra obtained during the titration of $[ZnL]$ with DTT. The inset shows a plot of absorbance vs $[DTT]/[ZnL]$ for different bands. ESI MS for $\{DTT\cdot Zn\}$ complex with its isotopic peak pattern: (b) observed and (c) calculated.

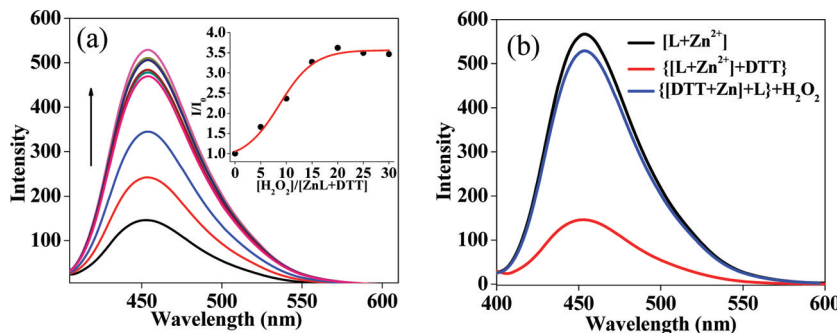


Figure 12. (a) Fluorescence spectra obtained during the titration of $\{[\text{DTT} + \text{Zn}^{2+}] + \text{L}\}$ with H_2O_2 in aqueous ethanol (1:2 v/v) containing HEPES buffer (pH = 7.4), $\lambda_{\text{ex}} = 390$ nm. The inset shows the relative fluorescence intensity (I/I_0) as a function of $[\text{H}_2\text{O}_2]/\{[\text{DTT} + \text{Zn}^{2+}] + \text{L}\}$ mole ratio. Note: the 30% H_2O_2 {1 mL in 2 mL buffer} has been diluted twice with buffer and used for the titrations. (b) Comparison of the fluorescence spectra for $[\text{L} + \text{Zn}^{2+}]$, $\{[\text{L} + \text{Zn}^{2+}] + \text{DTT}\}$, and $\{[\text{DTT} + \text{Zn}^{2+}] + \text{L} + \text{H}_2\text{O}_2\}$.

important for the removal process. This indeed results in the fluorescence quenching, and the final fluorescence is similar to that exhibited by L, since the Zn^{2+} complex of Cys or DTT do not contribute to the fluorescence.

Under the UV light, the solutions of $[\text{ZnL}]$ were found to be nonfluorescent in the case of Cys and DTT, weakly fluorescent in the case of GSH, and highly fluorescent {like that of the $[\text{ZnL}]$ } in the presence of the other $-SH$ -containing molecules (Figure 10b, inset). The fluorescent or nonfluorescent behavior observed in the presence of these $-SH$ -containing molecules clearly support the release of Zn^{2+} and L from the $[\text{ZnL}]$ mainly in the case of Cys and DTT, partly in the case of GSH, and not at all with the other $-SH$ molecules. Therefore, this clearly distinguishes those capable molecules which can remove Zn^{2+} from $[\text{ZnL}]$ and release L, viz. Cys and DTT, from the rest of the $-SH$ molecules as can be noted from eq 1.

Absorption Titrations. The release of L from $[\text{ZnL}]$ by Cys or DTT has been supported even from the absorption titration studies. The absorbance of the ~ 380 nm band decreases and the new bands observed in the presence of Cys or DTT at ~ 325 and ~ 430 nm, corresponding to the free receptor L increases (Figure 11a; for others see Supporting Information, Figure S15) as a function of the concentration of the added Cys or DTT. However, the other $-SH$ -containing molecules do not show significant change in the absorbance of the 380 nm band and 325 and 430 nm bands. Therefore, the changes observed in case of Cys or DTT are attributable to the displacement of Zn^{2+} from $[\text{ZnL}]$ and the complexation of the released Zn^{2+} by Cys or DTT (Figure 11a).

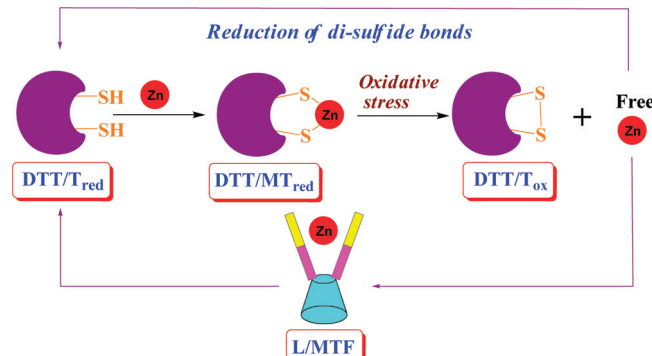
ESI MS Titration of $[\text{ZnL}]$ with Cys and DTT. The complex species of Cys or DTT formed with the freed Zn^{2+} has been shown by ESI MS through the observation of the peaks at 1382.29 for $(\text{L} + \text{H})$ and 338.75 for $(2\text{Cys} + \text{Zn} + \text{CH}_3\text{OH} + \text{H}_2\text{O} + 2\text{Na}^+)$ and 371.90 for $(2\text{DTT} + \text{Zn} + 2\text{H})$ (Figure 11b,c and Supporting Information, Figure S16). Therefore, the changes observed in the titration of Cys or DTT are attributable to the release of Zn^{2+} and L from the $[\text{ZnL}]$ followed by the complexation of Zn^{2+} by Cys or DTT. Both the absorption and fluorescence spectral studies clearly demonstrate the release of L from $[\text{ZnL}]$ upon titration with Cys or DTT.

C. Oxidative Stress and Heavy Metal Toxicity Events: An Attempt To Mimic These by $[\text{ZnL}]$. Zn^{2+} is released from the metallothionein during the oxidative stress and heavy metal detoxification pathways. The elevated concentration of Zn^{2+} is responsible for various infections and diseases. In order

to understand the biochemical mechanism of zinc release from MT during oxidative stress and metal detoxification process, it is necessary to model this process by using *in vitro* biomimetic molecular systems. The sulfhydryl-containing organic molecule DTT has been used as a model in the present study which can be a better mimic of MT, and the conjugate L has been used as fluorescent probe for Zn^{2+} .

Fluorescence and Absorption Titrations of $[\text{ZnL}] + \text{DTT}$ with H_2O_2 . The titration of $[\text{ZnL}]$ with DTT results in the formation of the zinc–DTT complex and releases L, and hence the corresponding mixture is denoted as $\{[\text{DTT} + \text{Zn}^{2+}] + \text{L}\}$. All this has been studied by fluorescence, absorption, and ESI MS. The fluorescence and absorption experiments were carried out with the model system, viz. $\{[\text{DTT} + \text{Zn}^{2+}] + \text{L}\}$ in the presence of the oxidizing agent, H_2O_2 , where the L probes the release of Zn^{2+} (through the changes observed in the fluorescence intensity) from the DTT complex. Upon the addition of H_2O_2 , the weakly fluorescent mixture, viz. $\{[\text{DTT} + \text{Zn}^{2+}] + \text{L}\}$, gains its full fluorescence intensity corresponding to the $[\text{ZnL}]$ (Figure 12). This is attributed to the oxidation of DTT and the consequent release of Zn^{2+} followed by its capture by L to form $[\text{ZnL}]$, which is highly fluorescent. These observations have been further substantiated based on the absorption study where the original band of the $[\text{ZnL}]$; i.e., 380 nm reappears upon the addition of H_2O_2 to a mixture of $\{[\text{DTT} + \text{Zn}^{2+}] + \text{L}\}$ (Scheme 2). Also noted was the oxidized

Scheme 2. Involvement of L as Zinc Recognition Element and DTT as Mimic to MT



product of DTT by H_2O_2 observed around ~ 238 nm, which has been further confirmed by carrying out a titration between simple DTT and H_2O_2 (Supporting Information, Figure S17).

Effect of Toxic Metal Ions (Cd^{2+} and Hg^{2+}) on Sensing of Cys and DTT by $[\text{ZnL}]$. During the heavy metal ion toxicity, the Zn^{2+} is freed from the metallothionein by sequestering Cd^{2+} or Hg^{2+} because these ions have high affinity of binding to the $-\text{SH}$ functions of MT_{red} . Indeed, Cys or DTT can act as small molecular mimic for MT_{red} . Therefore, this pathway has been modeled in the present case by carrying out the fluorescence titrations of a mixture of $\{[\text{Zn}(\text{Cys}/\text{DTT})] + \text{L}\}$ by $\text{Cd}^{2+}/\text{Hg}^{2+}$ and found to regain the fluorescence enhancement upon the addition of the heavy metal ions, which is equivalent to that of the $[\text{ZnL}]$ (Figure 13). The fluorescence data clearly fit well

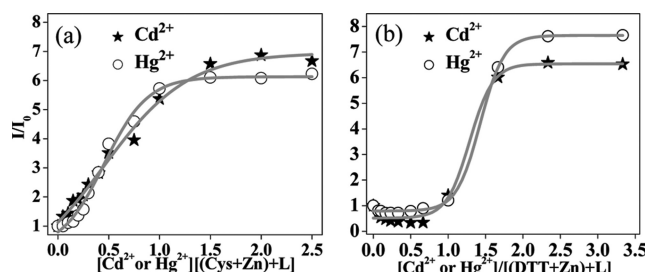


Figure 13. Relative fluorescence intensity plots obtained during the titration of $[\text{ZnL} + \text{Cys}/\text{DTT}]$ with Cd^{2+} or Hg^{2+} in aqueous ethanol (1:2 v/v) HEPES buffer ($\text{pH} = 7.4$), $\lambda_{\text{ex}} = 390 \text{ nm}$: (a) in the case of $\{\text{Zn}(\text{Cys}) + \text{L}\}$; (b) in the case of $\{\text{Zn}(\text{DTT}) + \text{L}\}$.

with the fact that the $[\text{Zn}(\text{Cys}/\text{DTT})]$ complex present in the mixture goes through a transmetalation by $\text{Cd}^{2+}/\text{Hg}^{2+}$, and thus the released Zn^{2+} forms a complex with L to exhibit fluorescence enhancement through the formation of $[\text{ZnL}]$ (Figure 13 and Supporting Information, Figure S18). These results were further confirmed by carrying out an absorption titration between the mixture, viz. $\{[\text{Zn}(\text{DTT/Cys})] + \text{L}\}$ by $\text{Cd}^{2+}/\text{Hg}^{2+}$, and the spectra supported the formation of $[\text{ZnL}]$ as well as the complex formed by $\text{Cd}^{2+}/\text{Hg}^{2+}$ with DTT/Cys (Supporting Information, Figures S19–S22).

The observed fluorescence enhancement of the $\{\text{Zn}(\text{Cys}/\text{DTT}) + \text{L}\}$ when titrated with Cd^{2+} or Hg^{2+} suggests the reformation of the $[\text{ZnL}]$ followed by the transfer of $\text{Cd}^{2+}/\text{Hg}^{2+}$ to Cys/DTT. Therefore, the data reveal the importance of MTs and free $-\text{SH}$ residues in the biological medium for the detoxification and sensing of heavy metal ions by using OFF and ON fluorescence of L and $[\text{ZnL}]$, respectively (Figure 14).

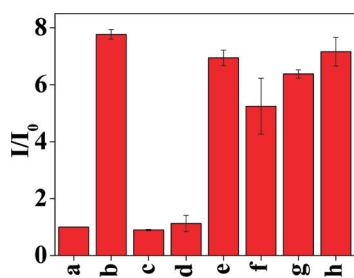
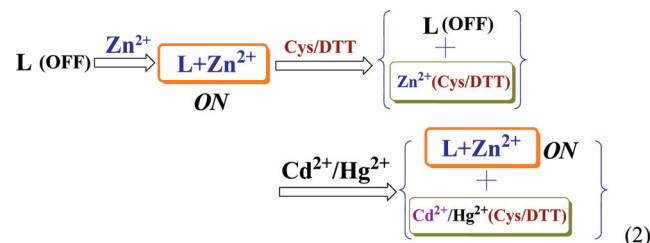


Figure 14. Histogram showing the relative fluorescence response of L in aqueous ethanol (1:2 v/v) HEPES buffer ($\text{pH} = 7.4$) solution in different condition: (a) L ; (b) $[\text{L} + \text{Zn}^{2+}]$; (c) $\{[\text{L} + \text{Zn}^{2+}] + \text{Cys}\}$; (d) $\{[\text{L} + \text{Zn}^{2+}] + \text{DTT}\}$; (e) $\{[\text{L} + \text{Zn}^{2+}] + \text{Cys}\} + \text{Cd}^{2+}$; (f) $\{[\text{L} + \text{Zn}^{2+}] + \text{Cys}\} + \text{Hg}^{2+}$; (g) $\{[\text{L} + \text{Zn}^{2+}] + \text{DTT}\} + \text{Cd}^{2+}$; (h) $\{[\text{L} + \text{Zn}^{2+}] + \text{DTT}\} + \text{Hg}^{2+}$.

ESI MS Titration of $\{\text{Zn}(\text{DTT}) + \text{L}\}$ with Cd^{2+} and Hg^{2+} . To provide further proof for the formation of the complexes

between $\text{Cd}^{2+}/\text{Hg}^{2+}$ and DTT/Cys, and the release of Zn^{2+} from the $[\text{Zn}(\text{DTT/Cys})]$, ESI MS titrations were carried out. The mass spectral data show the peaks at m/z 446.73 for $(2\text{Cys} + \text{Cd} + \text{CH}_3\text{OH} + \text{H}^+)$, 440.89 for $(2\text{Cys} + \text{Hg} + 2\text{H}^+)$, and 419.90 for $(2\text{DTT} + \text{Cd} + 3\text{H} + \text{Na}^+)$, 434.92 for $(\text{DTT} + \text{Hg} + 2\text{CH}_3\text{OH} + 2\text{H}_2\text{O})$ (Supporting Information, Figures S23–S26). All this clearly support the displacement of zinc from $[\text{Zn}(\text{DTT/Cys})]$ by Cd^{2+} or Hg^{2+} as shown through eq 2.



CONCLUSIONS AND CORRELATIONS

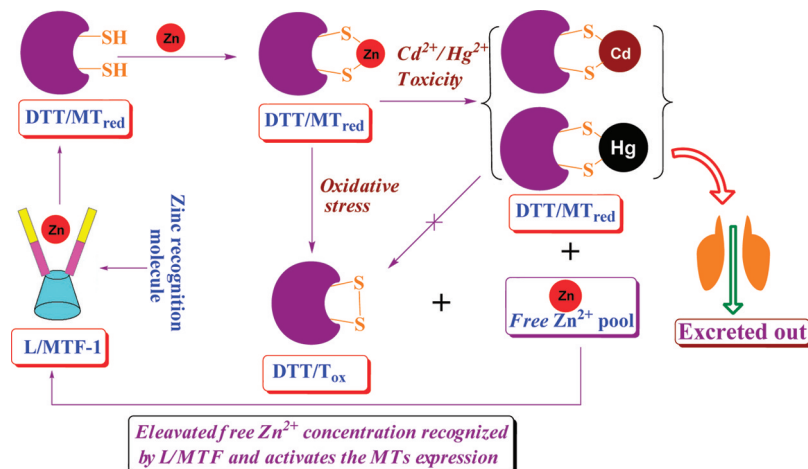
Development of a synthetic organic molecular model system that can provide us with some clues on the complex nature of the oxidative stress and the heavy metal ion detoxification process would indeed be a welcome feature of the bioinorganic chemistry of metallothioneins. A suitably modified supramolecular calix[4]arene system (L) has been developed as the sensitive and selective recognition tool for Zn^{2+} . The high sensitivity and selectivity of L toward Zn^{2+} has been demonstrated on the basis of the fluorescence, absorption, and ESI-MS and also by visual fluorescent color change. The structural, electronic, and emission properties of the calix[4]-arene conjugates L and its zinc complex, $[\text{ZnL}]$, have been demonstrated using DFT computational calculations. L can detect Zn^{2+} up to $47 \pm 8 \text{ ppb}$ ($718 \pm 122 \text{ nM}$) by *switch on* fluorescence, suggesting its applicability to detect Zn^{2+} ions in aqueous medium at physiological conditions. Therefore, L can be used as a sensitive and selective *switch on* fluorescence receptor for Zn^{2+} . The TDDFT calculations reveal that the *switch on* fluorescence behavior of L is mainly due to the utilization of the lone pair of electrons on imine moiety by the Zn^{2+} . The resultant fluorescent $[\text{ZnL}]$ has been used as a secondary chemosensor ensemble for the detection of $-\text{SH}$ -containing molecules.

In the presence of Cys or DTT, the Zn^{2+} is being freed from $[\text{ZnL}]$ and is complexed by Cys or DTT, as demonstrated by a combination of different techniques. The displacement followed by the release of the coordinated zinc from its Cys/DTT complex by heavy metal ion (viz. Cd^{2+} or Hg^{2+}), as in the metal detoxification pathway or by ROS (such as H_2O_2) as in the oxidative stress (Scheme 3), has been well demonstrated by the L . The L in turn mimics the zinc sensing element (MTF) in biology. Therefore, to our knowledge, this is the first report of a synthetic calix[4]arene conjugate that mimics some critical steps of the metal detoxification and oxidative stress events noticed in biology, in which metallothionein plays a central role.

EXPERIMENTAL SECTION

General Information and Materials. All the perchlorate salts, viz. $\text{NaClO}_4 \cdot \text{H}_2\text{O}$, KClO_4 , $\text{Ca}(\text{ClO}_4)_2 \cdot 4\text{H}_2\text{O}$, $\text{Mg}(\text{ClO}_4)_2 \cdot 6\text{H}_2\text{O}$, $\text{Mn}(\text{ClO}_4)_2 \cdot 6\text{H}_2\text{O}$, $\text{Fe}(\text{ClO}_4)_2 \cdot x\text{H}_2\text{O}$, $\text{Co}(\text{ClO}_4)_2 \cdot 6\text{H}_2\text{O}$, $\text{Ni}(\text{ClO}_4)_2 \cdot 6\text{H}_2\text{O}$, $\text{Cu}(\text{ClO}_4)_2 \cdot 6\text{H}_2\text{O}$, $\text{Hg}(\text{ClO}_4)_2 \cdot 4\text{H}_2\text{O}$, $\text{Zn}(\text{ClO}_4)_2 \cdot 6\text{H}_2\text{O}$, and $\text{Cd}(\text{ClO}_4)_2 \cdot \text{H}_2\text{O}$, and different thiols, viz. Cys,

Scheme 3. Schematic Representation of the Events Involving the Heavy Metal Toxicity and Oxidative Stress Wherein the DTT Mimics MTs and L Mimics the Zinc Recognition Element^a



^aCd²⁺ and Hg²⁺ have been used as heavy metals and H₂O₂ as oxidant.

DTT, GSH, MPA, Hcy, ME, and Cyst, were purchased from the commercial suppliers in India and the US. All the fluorescence titrations were carried out in 1 cm quartz cells by using 50 μ L of L, and the total volume in each measurement was made to 3 mL to give a final concentration of the ligand as 10 μ M. The fluorescence studies performed in aqueous ethanolic HEPES buffer, pH = 7.4 solution used always a 50 μ L of bulk solution of L prepared at 6×10^{-4} M concentration in ethanol. A 50 mM HEPES buffer stock solution was prepared with deionized water, and 1000 μ L of this bulk solution is used for each titration of 3 mL solution. During the titration, the concentration of the metal perchlorate has been varied accordingly to result in requisite mole ratios of metal ion to L, and the total volume of the solution was maintained at 3 mL in each case by addition of aqueous ethanol. For absorption studies, the final concentration of [L] was kept constant at 10 μ M, and the procedure used for the titrations was the same as that used for fluorescence titrations. The *in situ* prepared zinc complex of L (L:Zn²⁺ = 1:2) has been used for the titration of [ZnL] with thiols. The mixture of {[DTT/Cys + Zn²⁺] + L} was again subjected to titration with Cd²⁺, Hg²⁺, and H₂O₂ (30%). The H₂O₂ (30%) {1 mL in 2 mL buffer} has been diluted by 2-fold with buffer and used for the oxidation titrations by adding directly.

Experimental for Computational Calculation of L and [ZnL]. The computational calculations were carried out to find the mode of complexation of Zn²⁺ with L. As the formation of 1:1 {L:Zn²⁺} species has already been established by the ESI-MS and supported by the Job's plot, the species was optimized by computational calculations based on DFT using Gaussian 03 package (Supporting Information). The initial model for L was prepared from the published^{11h} crystal data of triazole-linked calix[4]arene conjugate by removing Zn²⁺ followed by the protonation of the salicyl OH moieties and further by introducing methylthiophene group in the place of *n*-butyl group in each of the arm. This is then optimized by going through a cascade process of computational calculations. Thus, L was optimized by going through PM3 \rightarrow HF/STO-3G \rightarrow HF/3-21G \rightarrow HF/6-31G \rightarrow B3LYP/3-21G \rightarrow B3LYP/6-31G in a cascade manner, and the complex was optimized using B3LYP/6-31G(d,p). The output obtained at every stage was given as the input for the next higher level of calculations. In order to make the neutral complex of L with Zn²⁺, the salicyl OH groups were deprotonated and the resulting L²⁻ was used for further studies. In order to reduce the computational times, the L²⁻ was converted to L²⁻ by replacing the tertiary butyl moieties with hydrogen. The Zn²⁺ complex of L²⁻ was made by placing the Zn²⁺ far away from this. After the optimization of [ZnL], NBO charges and single-excitation time-dependent DFT (TDDFT) calculations were performed.

Synthesis and Characterization of 1.¹⁴ SnCl₄ (1.07 g, 4.1 mmol) was added to a solution containing *p*-*tert*-butylphenol (6.01 g, 40 mmol) in dry toluene. Bu₃N was added dropwise to the above reaction mixture and stirred the solution for 20 min. To the reaction mixture, paraformaldehyde (2.43 g, 81 mmol) was added and heated to reflux for 8 h. After cooling the reaction mixture to room temperature, the solution was poured into a separating funnel and then extracted with diethyl ether (2 \times 50 mL). The combined organic layer was washed with saturated sodium chloride and dried over anhydrous sodium sulfate. The product formed was purified by silica gel column chromatography using petroleum ether and ethyl acetate. Yield (4.5 g, 63%). ¹H NMR (CDCl₃, δ ppm): 1.25 (s, 9H), 6.86 (s, 1H, *J* = 9.1 Hz), 7.44 (d, 1H, *J* = 2.4 Hz), 7.52 (dd, 1H, *J* = 2.4 Hz), 9.82 (s, 1H), 10.80 (s, 1H).

Synthesis and Characterization of 2.¹⁴ To a mixture of 1 (5.0 g, 28 mmol) and 35% formaldehyde (25 mL) was added 125 mL of concentrated HCl and stirred the solution for 2 days at room temperature. Water was added to the mixture, the product was extracted into CH₂Cl₂ (3 \times 40 mL), and the organic phase was dried over anhydrous Na₂SO₄. The CH₂Cl₂ was then evaporated under reduced pressure to afford the pure product as yellow liquid. Yield (5.2 g, 82%). ¹H NMR (CDCl₃): 1.34 (s, 9H), 4.70 (s, 2H), 7.52 (d, 1H, *J* = 2.4 Hz), 7.67 (d, 2H, *J* = 2.5 Hz), 9.90 (s, 1H), 11.28 (s, 1H).

Synthesis and Characterization of L₂.^{11h} Compound 2 (2.65 g, 11.89 mmol) was added to a solution of sodium azide (1.519 g, 23.37 mmol) in 30 mL of dimethylformamide under stirring for 12 h. After completion of reaction mixture was diluted with 100 mL of water and ethyl acetate. The organic layer was separated and washed with water and brine. A yellow liquid was obtained upon evaporation of organic solvent. Yield: 89%. ¹H NMR (CDCl₃, 400 Hz): 11.2 (br s, 1H), 9.99 (s, 1H), 7.55 (dd, 1H), 7.59 (s, 1H), 4.48 (s, 2H), 1.35 (s, 9 H). IR: ν_{max} = 3471, 2961, 2686, 2104, 1676.

Synthesis and Characterization of L₁.^{11h} A mixture of potassium carbonate (5.10 g, 36.72 mmol) and *p*-*tert*-butylcalix[4]-arene (10.0 g, 15.43 mmol) in dry acetone (200 mL) was stirred at room temperature for 1 h. A solution of propargyl bromide (6.49 g, 30.80 mmol) in dry acetone (50 mL) was added dropwise into the above stirred mixture over a period of 30 min. The reaction mixture was refluxed for 24 h and was then allowed to cool to room temperature. The reaction mixture was filtered over Celite to remove insoluble particles, and the filtrate was concentrated by a rotatory evaporator. 100 mL of 2 M HCl was added to the concentrated reaction mixture, and the product was extracted with dichloromethane (3 \times 100 mL). The combined organic extract was successively washed with water and brine (100 mL), dried over anhydrous Na₂SO₄, filtered, and evaporated to dryness in *vacuo*. The crude product was

recrystallized from $\text{CH}_2\text{Cl}_2/\text{CH}_3\text{OH}$ to afford **2** as a white solid (9.10 g, 82% yield). ^1H NMR (400 MHz, CDCl_3) δ (ppm): 7.07 (s, 4H), 6.73 (s, 4H), 6.50 (s, 2H), 4.74 (d, J = 2.4 Hz, 4H), 4.37 (d, J = 13.4 Hz, 4H), 3.33 (d, J = 13.4 Hz, 4H), 2.54 (t, J = 2.4 Hz, 2H), 1.30 (s, 18H), 0.90 (s, 18H). HRMS m/z Calcd for $\text{C}_{50}\text{H}_{60}\text{O}_4$: (M + H)⁺ 725.4570. Found 725.4576.

Synthesis and Characterization of L₃.^{11h} Compound **L₁** (3.0 g, 4.14 mmol) was added to the solution of **L₂** (2.12 g, 9.53 mmol) in 100 mL of dichloromethane and water (50:50) mixture. To this solution, $\text{CuSO}_4 \cdot 5\text{H}_2\text{O}$ (124.04 g, 0.50 mmol) and sodium ascorbate (328.0 mg, 1.70 mmol) were added. The resulting solution was stirred for 12 h at room temperature. Upon completion of the reaction as checked based on TLC, the organic layer was separated and the aqueous layer was extracted with dichloromethane (2×50 mL). The combined organic layer was washed with water and then with brine (2×100 mL) and dried over anhydrous Na_2SO_4 , and the solvent was removed under vacuo. The crude product was purified by triturating with hexane followed by filtering the precipitate. Yield: 89.91%. ^1H NMR (CDCl_3 , 400 MHz) δ (ppm): 11.30 (s, 2H), 9.83 (s, 2H), 8.08 (s, 2H), 7.62 (s, 2H), 7.49 (d, 2H), 7.15 (s, 2H), 6.98 (s, 4H), 6.77 (s, 4H), 5.56 (s, 2H), 5.18 (s, 2H), 4.14 (d, J = 13.0 Hz, 4H), 3.17 (d, J = 13.0 Hz, 4H), 1.27 (s, 18H), 1.26 (s, 18H), 0.96). ^{13}C NMR (CDCl_3 , 100 MHz) δ (ppm): 196.6, 157.1, 150.4, 149.6, 147.2, 144.2, 143.2, 141.5, 135.3, 132.6, 130.7, 127.8, 125.6, 125.0, 124.2, 123.1, 120.2, 69.8, 48.2, 34.2, 33.9, 33.8, 31.7, 31.2, 31.1, 31.02. IR: ν = 3463, 2959, 1656, 1483, cm^{-1} . HRMS (ESI) calcd for $\text{C}_{74}\text{H}_{90}\text{N}_6\text{O}_8$ [M + H]⁺: 1191.6898; found 1191.6898.

Synthesis and Characterization of L. The mixture of **L₃** (0.25 g, 0.209 mmol) and the thiophen-2-ylmethanamine (0.047 g, 0.419 mmol) in 5 mL of methanol was stirred for 5 h. A faint yellow precipitate was observed upon completion of reaction. The precipitate was filtered to get yellow solid product. Yield: 93%. ^1H NMR (CDCl_3 , 400 MHz): 13.56 (s, 2H), 8.34 (s, 2H), 8.10 (s, 2H), 7.42 (d, 4H), 7.22–7.23 (m, 4H, Sal-H), 7.12 (s, 2H), 6.97 (s, 4H), 6.96 (s, 4H), 6.74 (s, 4H), 5.58 (S, 2H), 5.16 (S, 2H), 4.87 (s, 4H), 4.15 (d, 4H), 3.14 (d, 4H), 1.27 (s, 18H), 1.25 (s, 18H), 0.944 (s, 18H). ^{13}C NMR (CDCl_3 , 100 MHz) δ (ppm): 165.78, 157.01, 150.58, 149.69, 147.04, 144.01, 141.63, 141.40, 144.30, 132.66, 130.85, 128.93, 127.88, 127.13, 125.75, 125.62, 125.26, 125.04, 124.29, 122.35, 118.18, 69.79, 56.97, 48.91, 34.09, 33.98, 33.88, 31.81, 31.44, 31.08, 30.51. HRMS (ESI) calcd for $\text{C}_{84}\text{H}_{100}\text{N}_8\text{O}_6\text{S}_2$ [M + H]⁺: 1381.7302; found 1381.7286.

ASSOCIATED CONTENT

Supporting Information

^1H and ^{13}C NMR mass spectral data, absorption data, and fluorescence data. This material is available free of charge via the Internet at <http://pubs.acs.org>.

AUTHOR INFORMATION

Corresponding Author

*Phone: 91 22 2576 7162. Fax: 91 22 2572 3480. E-mail: cprao@iitb.ac.in.

ACKNOWLEDGMENTS

C.P.R. acknowledges the financial support from DST, CSIR, and DAE-BRNS. R.K.P. acknowledges CSIR and M.M. acknowledges UGC for their fellowships.

REFERENCES

- (a) Palmeter, R. D. *Proc. Natl. Acad. Sci. U. S. A.* **1998**, *95*, 8428. (b) Blaudauer, C. A.; Leszczyszyn, O. I. *Nat. Prod. Rep.* **2010**, *27*, 720. (c) Krezel, A.; Maret, W. *Biochem. J.* **2007**, *402*, 551. (d) Nordberg, M.; Nordberg, G. F. *Met. Ions Life Sci.* **2009**, *5*, 1. (e) Krezel, A.; Maret, W. *J. Am. Chem. Soc.* **2007**, *129*, 10911.
- (a) Maret, W. *Proc. Natl. Acad. Sci. U. S. A.* **1994**, *91*, 237. (b) Carpene, E.; Andreani, G.; Isani, G. *J. Trace Elem. Med. Biol.* **2007**, *21*, 35. (c) Coyle, P.; Philcoxa, J. C.; Careya, L. C.; Rofea, A. M. *Cell Mol. Life Sci.* **2002**, *59*, 627. (d) Palmeter, R. D. *Proc. Natl. Acad. Sci. U. S. A.* **2004**, *101*, 4918. (e) Ercal, N.; Gurer-Orhan, H.; Aykin-Burns, N. *Curr. Top. Med. Chem.* **2001**, *1*, 529.
- (a) Colvin, R. A.; Holmes, W. R.; Fontaine, C. P.; Maret, W. *Metalomics* **2010**, *2*, 306. (b) Aizenman, E.; Stout, A. K.; Hartnett, K. A.; Dineley, K. E.; McLaughlin, B.; Reynolds, I. *J. J. Neurochem.* **2000**, *75*, 1878.
- (a) Chang, C. J.; Jaworski, J.; Nolan, E. M.; Sheng, M.; Lippard, S. J. *Proc. Natl. Acad. Sci. U. S. A.* **2004**, *101*, 1129. (b) Maret, W. *Biochemistry* **2004**, *43*, 3301.
- (a) Flora, S. J. S.; Mittal, M.; Mehta, A. *Indian J. Med. Res.* **2008**, *128*, 501. (b) Hall, J. L. *J. Exp. Bot.* **2002**, *53*, 1. (c) Maret, W. *Biometals* **2010**, *24*, 411. (d) Ejnik, J.; Shaw, C. F.; Petering, D. H. *Inorg. Chem.* **2010**, *49*, 6525.
- (a) Smirnova, I. V.; Bittel, D. C.; Ravindra, R.; Jiang, H.; Andrews, G. K. *J. Biol. Chem.* **2000**, *275*, 9377. (b) Haase, H.; Rink, L. *Annu. Rev. Nutr.* **2009**, *29*, 133.
- (a) Li, Y.; Hawkins, B. E.; DeWitt, D. S.; Prough, D. S.; Maret, W. *Brain Res.* **2010**, *1330*, 131. (b) Sensi, S. L.; Paoletti, P.; Bush, A. I.; Sekler, I. *Nat. Rev. Neurosci.* **2009**, *10*, 780. (c) Mei, Y.; Frederickson, C. J.; Giblin, L. J.; Weiss, J. H.; Medvedeva, Y.; Bentley, P. A. *Chem. Commun.* **2011**, *47*, 7107. (d) Tomat, E.; Lippard, S. J. *Curr. Opin. Chem. Biol.* **2010**, *14*, 225. (e) Domaille, D. W.; Que, E. L.; Chang, C. J. *Nat. Chem. Biol.* **2008**, *4*, 168. (f) Komatsu, K.; Urano, Y.; Kojima, H.; Nagano, T. *J. Am. Chem. Soc.* **2007**, *129*, 13447.
- (a) Steed, J. W. *Science* **2002**, *298*, 976. (b) Reinhoudt, D. N.; Crego-Calama, M. *Science* **2002**, *295*, 2403. (c) Izett, G.; Zeitouny, J.; Akdas-Killig, H.; Frapart, Y.; Menage, S.; Douziech, B.; Jabin, I.; Le Mest, Y.; Renaud, O. *J. Am. Chem. Soc.* **2008**, *130*, 9514. (d) Le Poul, N.; Douziech, B.; Zeitouny, J.; Thiabaud, G.; Colas, H.; Conan, F.; Cosquer, N.; Jabin, I.; Lagrost, C.; Hapiot, P.; Reinaud, O.; Le Mest, Y. *J. Am. Chem. Soc.* **2009**, *131*, 17800. (e) Seneque, O.; Rager, M.-N.; Giorgi, M.; Prange, T.; Tomas, A.; Reinaud, O. *J. Am. Chem. Soc.* **2005**, *127*, 14833. (f) Perret, F.; Lazar, A. N.; Coleman, A. W. *Chem. Commun.* **2006**, 2425.
- (a) Cacciapaglia, R.; Casnati, A.; Mandolini, L.; Reinhoudt, D. N.; Salvio, R.; Sartori, A.; Ungaro, R. *J. Am. Chem. Soc.* **2006**, *128*, 12322. (b) Cacciapaglia, R.; Casnati, A.; Mandolini, L.; Reinhoudt, D. N.; Salvio, R.; Sartori, A.; Ungaro, R. *J. Org. Chem.* **2005**, *70*, 624. (c) Cacciapaglia, R.; Casnati, A.; Mandolini, L.; Reinhoudt, D. N.; Salvio, R.; Sartori, A.; Ungaro, R. *J. Org. Chem.* **2005**, *70*, 5398. (d) Bakirci, H.; Koner, A. L.; Dickman, M. H.; Kortz, U.; Nau, W. M. *Angew. Chem., Int. Ed.* **2006**, *45*, 7400. (e) Ozturk, G.; Akkaya, E. U. *Org. Lett.* **2004**, *6*, 241. (f) Park, S. Y.; Yoon, J. H.; Hong, C. S.; Souane, R.; Kim, J. S.; Matthews, S. E.; Vicens, J. *J. Org. Chem.* **2008**, *73*, 8212. (g) Senthilvelan, A.; Ho, I.-T.; Chang, K.-C.; Lee, G.-H.; Liu, Y.-H.; Chung, W.-S. *Chem.—Eur. J.* **2009**, *15*, 6152. (h) Bagatin, I. A.; de Souza, E. S.; Ito, A. S.; Toma, H. E. *Inorg. Chem. Commun.* **2003**, *6*, 288. (i) Jiang, P.; Guo, Z. *Coord. Chem. Rev.* **2004**, *248*, 205. (j) Kumar, M.; Kumar, R.; Bhalla, V. *Org. Lett.* **2011**, *13*, 366.
- (a) Valeur, B.; Leray, I. *Coord. Chem. Rev.* **2000**, *205*, 3. (b) Leray, I.; Valeur, B. *Eur. J. Inorg. Chem.* **2009**, 3525. (c) Kim, J. S.; Lee, S. Y.; Yoon, J.; Vicens, J. *Chem. Commun.* **2009**, 4791. (d) de Silva, A. P.; Gunaratne, H. Q. N.; Gunnlaugsson, T.; Huxley, A. J. M.; McCoy, C. P.; Rademacher, J. T.; Rice, T. E. *Chem. Rev.* **1997**, *97*, 1515. (e) Chang, K.-C.; Su, I.-H.; Lee, G.-H.; Chung, W.-S. *Tetrahedron Lett.* **2007**, *48*, 7274. (f) Chang, K.-C.; Su, I.-H.; Senthilvelan, A.; Chung, W.-S. *Org. Lett.* **2007**, *9*, 3363. (g) Chang, K.-C.; Su, I.-H.; Wang, Y.-Y.; Chung, W.-S. *Eur. J. Org. Chem.* **2010**, 4700.
- (a) Kim, S. K.; Lee, S. H.; Lee, J. Y.; Bartsch, R. A.; Kim, J. S. *J. Am. Chem. Soc.* **2004**, *126*, 16499. (b) Schatzmann, B.; Alhashimy, N.; Diamond, D. *J. Am. Chem. Soc.* **2006**, *128*, 8607. (c) Kolusheva, S.; Zadmard, R.; Schrader, T.; Jelinek, R. *J. Am. Chem. Soc.* **2006**, *128*, 13592. (d) Filby, M. H.; Dickson, S. J.; Zaccheroni, N.; Prodi, L.; Bonacchi, S.; Montalti, M.; Paterson, M. J.; Humphries, T. D.; Chiorboli, C.; Steed, J. W. *J. Am. Chem. Soc.* **2008**, *130*, 4105. (e) He, X.; Yam, W. W. *Org. Lett.* **2011**, *13*, 2172. (f) Ni, X.-L.; Wang, S.; Zeng, X.; Tao, Z.; Yamato, T. *Org. Lett.* **2010**, *13*, 552. (g) Diamond, D. *Chem. Soc. Rev.* **1996**, *15*. (h) Pathak, R. K.; Dikundwar, A. G.;

Guru Row, T. N.; Rao, C. P. *Chem. Commun.* **2010**, *46*, 4345.
(i) Pathak, R. K.; Ibrahim, S. M.; Rao, C. P. *Tetrahedron Lett.* **2009**, *50*, 2730. (j) Joseph, R.; Rao, C. P. *Chem. Rev.* **2011**, *111*, 4658. (k) Kim, J. S.; Quang, D. T. *Chem. Rev.* **2007**, *107*, 3780.

(12) (a) Xu, Z.; Yoon, J.; Spring, D. R. *Chem. Soc. Rev.* **2010**, *39*, 1996. (b) Creaven, B. S.; Donlon, D. S.; McGinley, J. *Coord. Chem. Rev.* **2009**, *253*, 893. (c) McGinley, J.; Walsh, J. M. D. *Inorg. Chem. Commun.* **2011**, *14*, 1018. (d) Ni, X.-L.; Zeng, X.; Redshaw, C.; Yamato, T. *J. Org. Chem.* **2011**, *76*, 5696. (e) Zhang, J. F.; Bhuniya, S.; Lee, Y. H.; Bae, C.; Lee, J. H.; Kim, J. S. *Tetrahedron Lett.* **2010**, *51*, 3719. (f) Sahin, O.; Yilmaz, M. *Tetrahedron* **2011**, *67*, 3501.

(13) (a) Rivero, I. A.; Gonzalez, T.; Diaz-Garcia, M. E. *Comb. Chem. High. Throughput. Screen.* **2006**, *9*, 535. (b) Sonn, K.; Pankratova, S.; Korshunova, I.; Zharkovsky, A.; Bock, E.; Berezin, V.; Kiryushko, D. *J. Neurosci. Res.* **2010**, *88*, 1074.

(14) (a) Wang, Q.; Wilson, C.; Blake, A. J.; Collinson, S. R.; Tasker, P. A.; Schroder, M. *Tetrahedron Lett.* **2006**, *47*, 8983. (b) Lambert, E.; Chabut, B.; Chardon-Noblat, S.; Deronzier, A.; Chottard, G.; Bousseksou, A.; Tuchagues, J.-P.; Laugier, J.; Bardet, M.; Latour, J.-M. *J. Am. Chem. Soc.* **1997**, *119*, 9424. (c) Shao, N.; Zhang, Y.; Cheung, S.; Yang, R.; Chan, W.; Mo, T.; Li, K.; Liu, F. *Anal. Chem.* **2005**, *77*, 7294. (d) Joseph, R.; Chinta, J. P.; Rao, C. P. *Inorg. Chem.* **2011**, *50*, 7050–7058.

(15) Frisch, M. J.; Trucks, G. W.; Schlegel, H. B.; Scuseria, G. E.; Robb, M. A.; Cheeseman, J. R.; Montgomery, J. A., Jr.; Vreven, T.; Kudin, K. N.; Burant, J. C.; Millam, J. M.; Iyengar, S. S.; Tomasi, J.; Barone, V.; Mennucci, B.; Cossi, M.; Scalmani, G.; Rega, N.; Petersson, G. A.; Nakatsuji, H.; Hada, M.; Ehara, M.; Toyota, K.; Fukuda, R.; Hasegawa, J.; Ishida, M.; Nakajima, T.; Honda, Y.; Kitao, O.; Nakai, H.; Klene, M.; Li, X.; Knox, J. E.; Hratchian, H. P.; Cross, J. B.; Adamo, C.; Jaramillo, J.; Gomperts, R.; Stratmann, R. E.; Yazyev, O.; Austin, A. J.; Cammi, R.; Pomelli, C.; Ochterski, J. W.; Ayala, P. Y.; Morokuma, K.; Voth, G. A.; Salvador, P.; Dannenberg, J. J.; Zakrzewski, V. G.; Dapprich, S.; Daniels, A. D.; Strain, M. C.; Farkas, O.; Malick, D. K.; Rabuck, A. D.; Raghavachari, K.; Foresman, J. B.; Ortiz, J. V.; Cui, Q.; Baboul, A. G.; Clifford, S.; Cioslowski, J.; Stefanov, B. B.; Liu, G.; Liashenko, A.; Piskorz, P.; Komaromi, I.; Martin, R. L.; Fox, D. J.; Keith, T.; Al-Laham, M. A.; Peng, C. Y.; Nanayakkara, A.; Challacombe, M.; Gill, P. M. W.; Johnson, B.; Chen, W.; Wong, M. W.; Gonzalez, C.; Pople, J. A. *Gaussian 03, revision C.02*; Gaussian, Inc.: Wallingford, CT, 2004.

(16) Mameli, M.; Aragoni, M.; Arca, M.; Caltagirone, C.; Demartin, F.; Farruggia, G.; De Filippo, G.; Devillanova, F.; Garau, A.; Isaia, F.; Lippolis, V.; Murgia, S.; Prodi, L.; Pintus, A.; Zaccheroni, N. *Chem.—Eur. J.* **2010**, *16*, 919.

(17) (a) Ko, C. K.; Wu, J. -S.; Kim, H. J.; Kwon, P. S.; Kim, J. W.; Bartsch, R. A.; Lee, J. Y.; Kim, J. S. *Chem. Commun.* **2011**, *47*, 3165. (b) Jung, H. S.; Ko, K. C.; Lee, J. H.; Kim, S. H.; Bhuniya, S.; Lee, J. Y.; Kim, Y.; Kim, S. J.; Kim, J. S. *Inorg. Chem.* **2010**, *49*, 8552. (c) Maity, D.; Manna, A. K.; Karthigeyan, D.; Kundu, T. K.; Pati, S. K.; Govindaraju, T. *Chem.—Eur. J.* **2011**, *17*, 11152.